JOURNAL OF GEOPHYSICAL RESEARCH, VOL. 112, C11018, doi:10.1029/2007JC004107, 2007

Three-dimensional shoaling of large-amplitude internal waves

V. Vlasenko[1] and N. Stashchuk[1]

Received 17 January 2007; revised 13 July 2007; accepted 20 August 2007; published 30 November 2007.

[1] The three-dimensional (3-D) shoaling of large-amplitude internal waves (LAIW) is studied in the framework of a fully nonlinear nonhydrostatic numerical model. The vertical fluid stratification, parameters of the propagating waves and bottom topography were taken close to those observed in the northern part of the Andaman Sea. It was found that three-dimensional evolution of LAIWs propagating from the deep part of a basin onto the shelf differs from two-dimensional shoaling in many ways largely because of the process of wave refraction developing in the areas of local bottom elevations or depressions. In the 3-D case the wave refraction produces concave and convex fragments of the wave fronts which may lead to the transverse redistribution of energy along the wave. Results demonstrate that concave wave fragments work as optical lenses focusing the wave energy to the centers of curvature. This process is especially important for LAIWs in shallow water zones where wave amplitudes are close to the saturation level. In general, the wave refraction leads to more fast wave breaking than that in the 2-D case. As a results, it should be expected to find localized regions of higher levels of water mixing and turbulence in the vicinity of local banks and headlands where LAIWs produce concave patterns. The areas of local bottom depressions, on the contrary, should be considered as potential places with lower level of background mixing.

Citation: Vlasenko, V., and N. Stashchuk (2007), Three-dimensional shoaling of large-amplitude internal waves, *J. Geophys. Res.*, *112*, C11018, doi:10.1029/2007JC004107.

1. Introduction

[2] Numerous in situ measurements and remote sensing observations reveal that tidally generated large amplitude internal waves (LAIW) are an ubiquitous phenomenon in the Global Ocean (see the reviews by *Ostrovsky and Stepanyants* [1989]; *Helfrich and Melville* [2006] and references therein). These waves, with their fronts extending for tens of kilometers may propagate several hundred kilometers from their source of generation carrying momentum and energy toward the coastline. As they shoal in shallow water near the coast, they can transport masses of water and the materials contained therein across isobaths. The transport of mass due to LAIWs plays an important role in some coastal marine ecosystems [*Leichter et al.*, 2003; *Pineda*, 1999; *Lennert-Cody and Franks*, 1999, 2002; *Helfrich and Pineda*, 2003]. LAIWs are potentially hazardous to all subsea operations including oil and gas drilling operations and have already caused several costly and dangerous incidents [*Fraser*, 1999].

[3] Several weakly nonlinear theories were developed to study shoaling of nonlinear internal waves. However, their application to LAIWs is under question owing to the strong nonlinearity of the latter. Various modifications of the Korteweg-de Vries (KdV) theories were used with some success to model wave evolution outside their formal range of validity [*Grimshaw et al.*, 1997; *Holloway et al.*, 1999; *Stanton and Ostrovsky*, 1998]. The extension of weakly nonlinear theory was completed also by *Miyata* [1985, 1988], *Choi and Camassa* [1999] and *Ostrovsky and Grue* [2003]. However, none of the models described above have been applied much beyond the solitary wave solutions. Another deficiency in most previous studies is that they treated oceanic LAIWs as a two-dimensional (2-D) phenomenon. In this respect, a purely 2-D wave may differ significantly from a 3-D one. For real oceanic conditions, it is difficult to apply the 2-D models without taking into account a number of spatial perturbing factors, such as radial spreading or 2-D depth variations.

[4] Various generalizations of the KdV equation have been suggested for nonlinear waves with smoothly curved phase fronts. One of the most popular is the Kadomtsev-Petviashvili equation. It was modified by *Grimshaw* [1985] [see also *Grimshaw and Tang*, 1990] to include weak transverse effect. An alternative approach to study spatial wave effects is the "nonlinear geometrical optics" approach, which describes refraction of wave fronts. This method, initially developed by *Ostrovsky and Shrira* [1976], was modified recently by *Small* [2001a] to study the refraction of planar internal wave obliquely propagating across a slope and Gaussian seamount [*Small*, 2001b].

[5] Some interesting 3-D effects may develop even in a 2-D configuration when a plane internal wave propagates

[1]School of Earth, Ocean and Environmental Sciences, University of Plymouth, Plymouth, UK.

0148-0227/07/2007JC004107$09.00

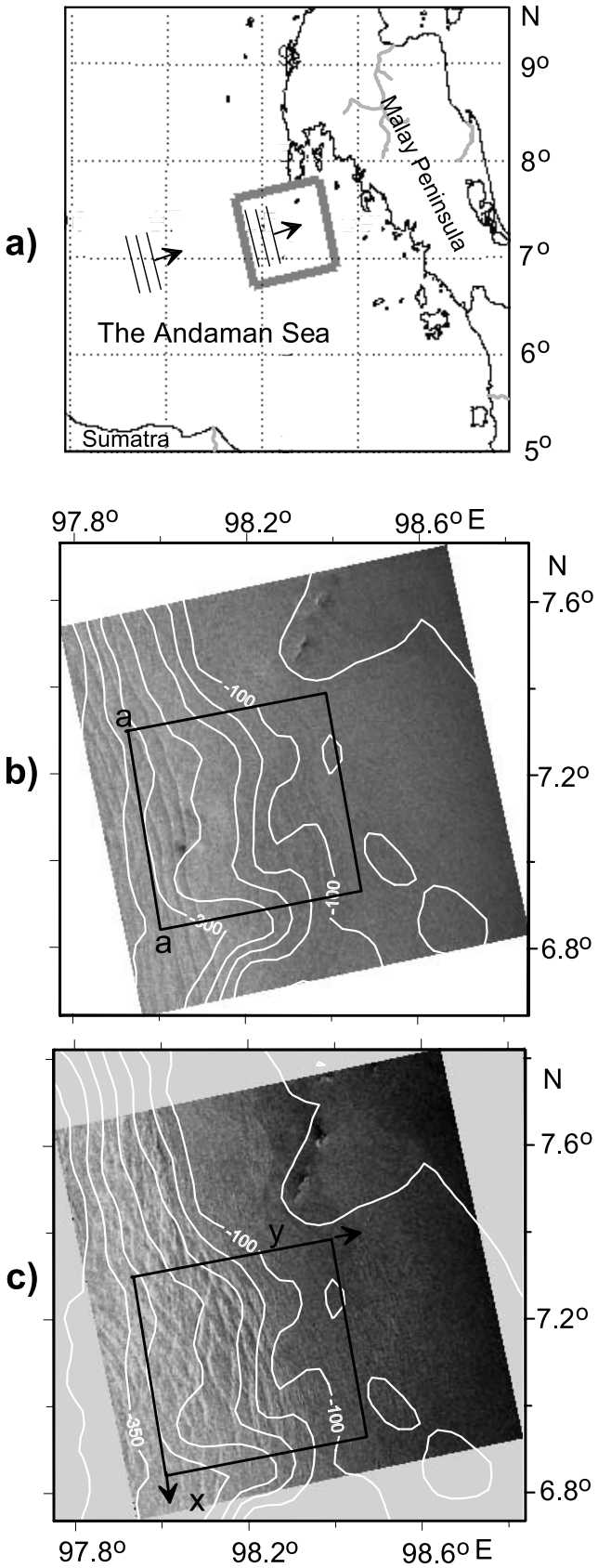

obliquely to the sloping bottom. As it was shown in series of papers by *Thorpe* [1987, 1997], an alongshore residual current is generated owing to the nonlinear reflection of internal wave from a slope. This current can be large enough to be registered by moored current meters, and this effect becomes stronger with the increase of the Coriolis parameter [*Thorpe*, 2000]. Such kind of effects should also be expected for LAIWs.

[6] Note however that the weakly nonlinear theories (even when modified and extended) cannot explain the strongly nonlinear effects occurring during interaction of internal waves with continental margins. There are a growing number of observations for which the weakly nonlinear approach is evidently wrong. This basically concerns the shelf-break areas where internal wave amplitude reaches the saturation level and where some other strongly nonlinear effects, such as wave breaking and water mixing take place. A more consistent description of the wave dynamics in such areas can be based on numerical simulation of the fully nonlinear hydrodynamic equations. Note, however, that 2-D numerical models such as developed by *Lamb* [2002, 2003] and *Vlasenko and Hutter* [2002a, 2002b] cannot be directly applied to the investigation of the shoaling of LAIWs in areas with substantial curvature of shelf bathymetry.

[7] An example of such a situation is shown in Figure 1 presenting a packet of tidally generated internal waves approaching the shelf-slope area in the Andaman Sea. The maritime regime of the Andaman Sea contains internal solitary waves of extraordinary amplitude (>60 m [see *Jackson*, 2004]). A group of LAIWs in the chosen area of the Andaman Sea normally propagates eastward (as presented in Figure 1a). *Alpers et al.* [1997], with the help of synthetic aperture radars (SAR) data, estimated that the most probable region of generation of the LAIWs presented in Figure 1 are the shallow reefs off the northwest coast of Sumatra, around 6°10′N, 95°0′E.

[8] In the place of wave shoaling (Figures 1b and 1c) the bottom topography has several headlands and canyons so that some 3-D effects of wave-bottom interaction may develop in the swash zone. Far from the shelf break where the packet of LAIWs is located at isobaths 300–400 m, the signature of the waves presents parallel lines (Figure 1b). Another SAR image taken in the very same place but several months later also represents a system of internal waves but these have penetrated much farther into the shallow water area (Figure 1c). This system does not reveal the well-organized structure but reveals a rather random 3-D pattern. The wave fragments are located much closer to the shelf break and their structure can presumably be treated as

Figure 1. (a) Fragment of the Andaman Sea with the gray rectangle showing the area with LAIWs. ERS synthetic aperture radar image acquired over the Andaman Sea during (b) orbit 24892 (frame 0135) on 18.03.96 at 1603 UTC and (c) orbit 23255 (frame 0135) on 1.11.99 at 1603 UTC showing surface manifestations of internal waves (courtesy of European Space Agency, 1996; acquired and processed by CRISP, Singapore). The white lines laid upon the images correspond to the bottom topography. The black rectangle shows the area being studied.

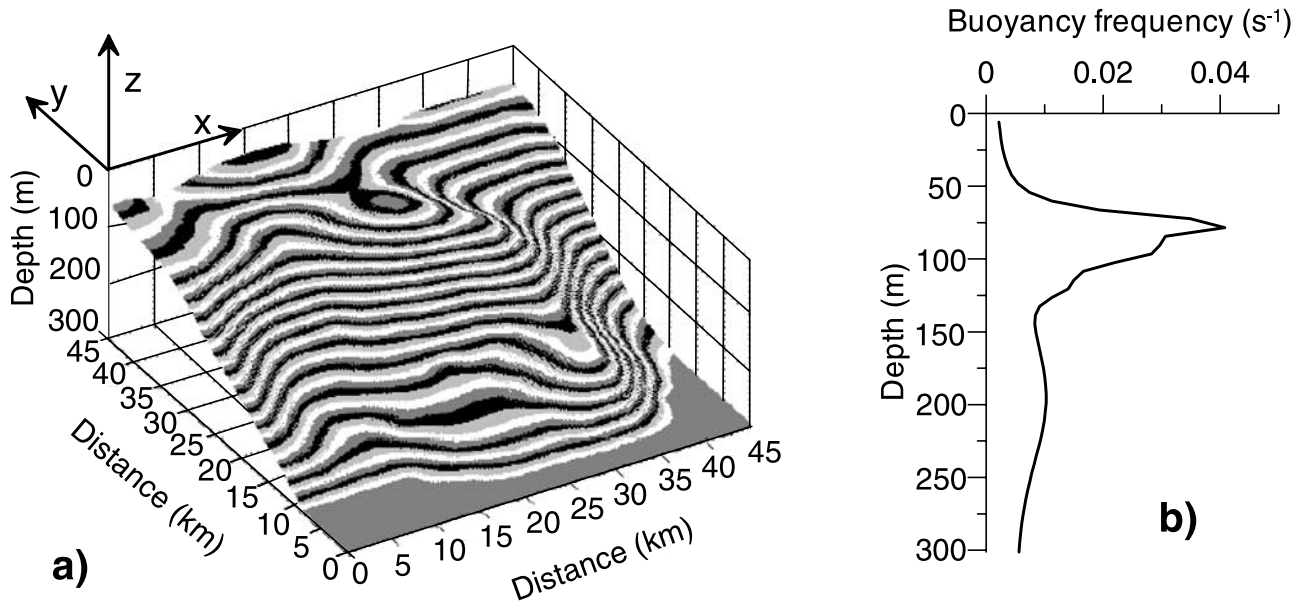

Figure 2. (a) Local bathymetry used in the model. (b) Typical winter buoyancy frequency profile.

a later stage of the scattering of a wave packet similar to that presented in Figure 1b on an irregular bottom topography.

[9] With the advent of satellites that carry high-resolution imaging systems, the growing number of similar evidence appears relating to the 3-D dynamics of LAIWs which should be adequately addressed in theory. Unfortunately, the 3-D dynamics of oceanic internal waves in the swash zone is still poorly understood. The breaking event and energy dissipation must be considered there as 3-D phenomena. The present paper is motivated by the intention to fill the gap in the understanding of the 3-D dynamics of oceanic internal waves at the more critical stage of their evolution, namely, disintegration, breaking and associated turbulent mixing. The focus is to apply a state-of-the-art numerical model to describe and quantify these processes in contrast to the traditional approach of looking at LAIWs as a 2-D phenomenon.

[10] The paper is organized as follows. The numerical model and its initialization are described in section 2. Section 3 presents the qualitative analysis of the basic case run and some implications resulting from the three-dimensionality of the experiment. The basic findings resulting from the comparison of 2-D and 3-D approaches are reported in section 4. The issues concerning energy balance are described in section 5. The results of sensitivity runs are discussed in section 6. A brief summary of the results are presented in the concluding section.

2. Model Description

[11] The evolution of LAIWs propagating in the Andaman Sea from Sumatra toward the Malay Peninsula (Figure 1a) is studied numerically. The model domain presented by the black rectangle in Figures 1b and 1c includes a 45 × 45 km^2 sector of irregular bottom topography. The three-dimensional projection of the bottom topography is also shown in Figure 2a. As it was mentioned above, the surface signature of the incoming LAIWs reveals quite a regular 2-D structure in the deep part of the sea with wave fronts parallel to the general direction of isobaths (see Figure 1b), whereas closer proximity to the shelf break (latest stage of evolution), the wave pattern manifests remarkable spatial anisotropy (see Figure 1c). Thus evidence of 3-D wave dynamics is clear, and the correct description of wave shoaling in the present case can be performed only in the framework of a 3-D approach.

[12] Consider the Cartesian system of coordinates $Oxyz$, with Oxy within the undisturbed free surface of the fluid and the Oz axis directed vertically upward. Here the x direction is along slope and the y direction is cross slope (see Figure 1c). The basin is filled with continuously stratified fluid whose stationary density profile $\rho(z)$ or its buoyancy frequency distribution $N(z)$, i.e., $N(z) = (-g/\rho \cdot \partial\rho/\partial z)^{1/2}$ is close to the climatic profile measured in the Andaman Sea in winter (see Figure 2b [*Levitus and Boyer*, 1994a, 1994b]). Here g is the acceleration due to gravity.

[13] It is assumed that the waves shown in Figures 1b and 1c are generated by the barotropic tide interacting with the shallow reefs (the area around 6°10′N, 95°0′E.). After generation, these waves propagate eastward from the Andaman Islands, and far from the source of generation they transform into wave packets, as schematically presented in Figure 1 (thin lines in Figure 1a). Note also that shoaling of such multiple wave groups normally produces quite irregular wave pattern in a shallow water zone (see for instance Figure 1c). In many cases this pattern includes a summary signal from many individual incident waves, which makes the correct interpretation of SAR images quite problematic. To simplify the study, let us consider the propagation of a single LAIW. It is obvious that the wave packet produces a more complicated pattern than that of a single solitary wave. However, in the first approximation this signal may be considered as a superposition of many elementary waves.

[14] In this study the problem of scattering of a plane LAIW on a 3-D bottom obstacle is split into two subtasks.

[15] 1. The first step is the model initialization, i.e., the preparation of the initial field of an incident LAIW. Generated near the Andaman Islands, internal waves propagate for about 400 km in the deep ocean before they arrive at the studied area. It is clear that all transition processes have been completed during such a long propagation and the incoming wave has transformed into a well developed stationary wave of depression. The influence of bottom topography during the deep-water propagation can be considered as negligible [*Vlasenko et al.*, 2005a].

[16] 2. The second stage of wave evolution is the shoaling process itself when the LAIW interacts with the abrupt three-dimensional obstacle presented in Figure 2a.

[17] For both problems the Massachusetts Institute of Technology general circulation model (MITgcm) was used; the detailed description of the model is presented in a paper by *Marshall et al.* [1997]. The MITgcm solves the nonhydrostatic, nonlinear equations and has a free surface formulation allowing it to trace the position of the solitary wave in (x, y) space.

[18] An initial 2-D LAIW of depression (the procedure of its definition is described below) is arranged in such a way as to be parallel to section $a - a$ (and x axis as well) at the depth of 300 m (see Figure 1b). The along-slope velocity is defined as u ($u = 0$ at $t = 0$), an across-slope counterpart is v, and w is the vertical component of a velocity vector. Taking into account the specific character of the model geometry with the orientation of the incident internal wave (and the general direction of isobaths) along the x axis, it was expected to find strong density and velocity gradients along the y axis, whereas x axis variations should be substantially weaker (at least at the first stage of wave shoaling). Several experiments have been carried out with the aim to define an optimum ratio $\Delta x/\Delta y$ which must be computer effective from one hand but in the same time which can provide correct reproduction of the wave refraction and does not introduce any computational (grid) effects. After some preliminary runs it was found that the best model resolution satisfying these controversial conditions is as follows: $\Delta x \times \Delta y \times \Delta z = 250$ m $\times$ 50 m $\times$ 6 m. It was found that further decrease of the ratio $\Delta x/\Delta y$ does not introduce any visible improvements.

[19] Assuming strong wave breaking and water mixing, we have chosen the Richardson number-dependent parameterizations [*Pacanowski and Philander*, 1981] of turbulent closure for viscosity ν and diffusivity κ, i.e.,

$$\nu = \frac{\nu_0}{(1+\beta \mathrm{Ri})^n} + \nu_b, \quad \kappa = \frac{\nu}{(1+\beta \mathrm{Ri})} + \kappa_b,$$

where Ri is the Richardson number, $\mathrm{Ri} = N^2(z)/(u_z^2 + v_z^2)$. Here $\nu_b = 10^{-3}$ m^{2}s^{-1} and $\kappa_b = 10^{-5}$ m^{2}s^{-1} are the background dissipation parameters, $\nu_0 = 1.5 \cdot 10^{-2}$ m^{2}s^{-1}, $\beta = 5$ and $n = 1$ are the adjustable parameters. Such a parameterization for the vertical turbulent viscosity ν and diffusivity κ increases their values in the areas where the Richardson number Ri is small. Horizontal diffusivity and viscosity were at the level of 0.1 m^{2}s^{-1}. As was found by *Vlasenko et al.* [2005b], with this parameterization the numerical model gives quite robust results even in the case of wave breaking. The open boundary conditions are used in the shelf and deep part of the domain; no flow along the slope direction and no slip at the topographic boundary are assumed [*Marshall et al.*, 1997].

[20] The procedure of preparation of the initial fields for an incident LAIW is described by *Vlasenko et al.* [2005b] in detail. Here we only briefly outline the basic stages. The model was initialized by the first-mode solitary wave of depression obtained from the KdV equation. Such an initial field represents a stationary weakly nonlinear solitary wave propagating in a nonhydrostatic medium. It does not however satisfies the fully nonlinear nonhydrostatic equations in the case of Large-amplitude waves which in the considered area should be more than 60 m [*Jackson*, 2004]. Thus, taking the amplitude of the initial KdV LAIW to be 75 m, which is far beyond the applicability of any weakly nonlinear models, we expect a substantial discrepancy with the hydrodynamic equations. Once inserted into the numerical scheme, a strong nonlinear KdV LAIW will evolve in a basin of constant depth. During this evolution the initial large-amplitude KdV solitary wave is modified, and a new stationary solitary wave is formed at the front of the wave field. The leading wave has the largest amplitude and, as a result, the largest phase speed. This is the reason why the largest wave detaches from the wave tail in the course of its evolution and propagates further as an independent internal solitary wave. The model is run until a leading wave separates from the wave tail. For the stratification shown in Figure 2b, the basic case run was performed with the LAIW having the amplitude of 69 m at the depth of 600 m.

3. Model Results

[21] The surface signature of internal waves as presented in Figure 1 is the result of the modulation of sea surface roughness due to the convergence/divergence produced by internal waves. These zones of strong vertical fluxes of ascending/descending water are located not directly in the center of the LAIW but at some distance from it. This means that black and white stripes in SAR images do not represent the real location of the wave. In fact the position of the wave crest (or trough) can be identified by the location of the depression (or elevation) produced by the internal wave at the free surface. For instance, a strong internal wave of depression with an amplitude of several tens of meters produces free surface elevation up to 0.1 m which is located just above the wave trough. The wave of elevation, on the contrary, produces a depression at the free surface of the same order. Although these distortions are pretty weak and can hardly be registered in the ocean directly by conventional measurement technique (only high-precision altimeters as used in TOPEX/Poseidon experiment

Figure 3. Sea surface topography produced by a LAIW at different stages of shoaling: (a) $t = 1$ hour 6 min, (b) $t = 2$ hours 13 min, (c) $t = 3$ hours 20 min, (d) $t = 4$ hours 26 min, (e) $t = 5$ hours 33 min, and (f) $t = 6$ hours 40 min. Surface elevations and depressions are shown by black and white colors, respectively. Thin solid lines represent the bottom topography. Arrows at the bottom of Figure 3c show the positions of vertical cross sections used in the analysis.

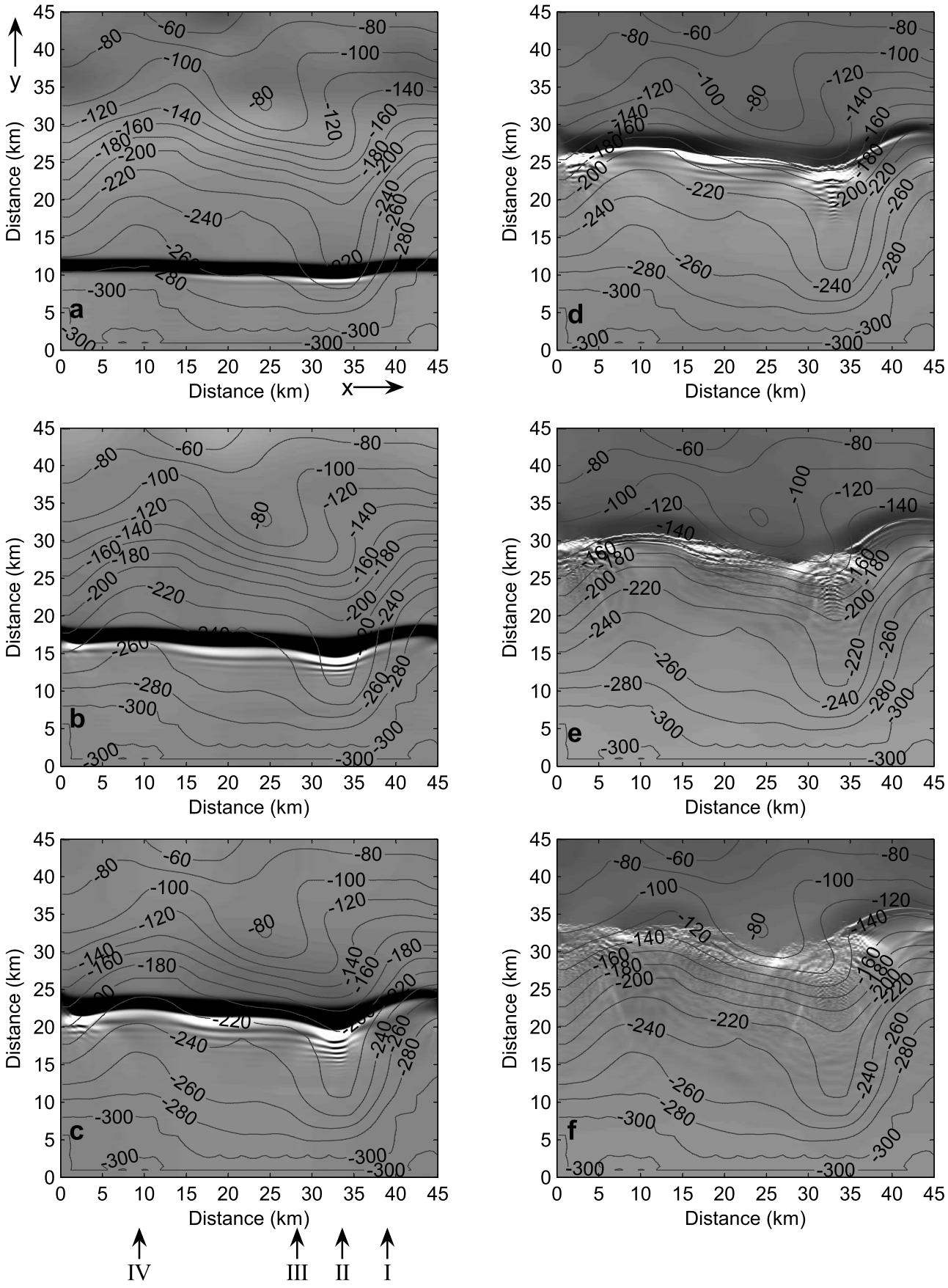

Figure 3

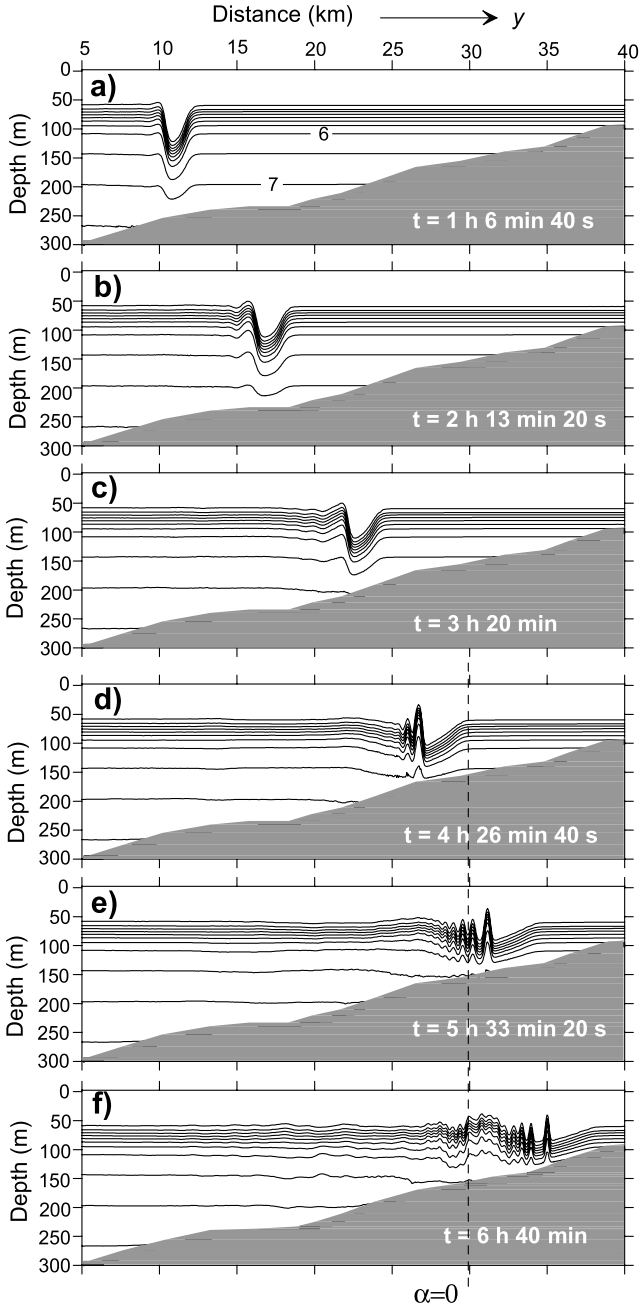

Figure 4. Time series presenting the density fields $\rho(z) - \rho(0)$ along section I (Figure 3) at different stages of wave evolution. Contour interval is equal to 0.5 kg m^{-3}. Vertical dashed line represents the position of the ''turning point'' where $\alpha = 0$.

can give the robust result [see *Egbert and Ray*, 2001]), this signal contains quite valuable information about the spatial characteristics of internal waves and can be considered in numerical modeling as a wave ''trace'' for the qualitative analysis of wave refraction and dispersion.

[22] Figure 3 represents a series of the sea surface topography produced by propagating a LAIW at different stages of shoaling. This signature is overlapped with the bottom topography. The black color corresponds to the free surface elevations produced by the internal waves of depression, whereas the white color represents the position of the negative free surface displacements generated by the internal waves of elevation. The gray background was chosen as an undisturbed zero level.

[23] As mentioned above, the numerical experiments were arranged in such a way as to reproduce the evolution of the LAIWs observed in the SAR images (see Figure 1). It was assumed that a plane LAIW of depression whose initial orientation of wave front is parallel to the Ox axis, is approaching the continental slope from the deep part of the sea and penetrates into a shallow water zone. The spatial (x, y) distribution of the basin's depth $H(x, y)$ was taken close to those observed in the studied area of the Andaman Sea (see Figure 1; the dashed rectangle there represents the computational domain).

[24] We start the analysis with Figure 3a, which shows the wave front one hour after the beginning of the numerical experiment. The black straight strip of approximately 2 km width reveals that the wave is still almost undisturbed in the area with average depth of about 300 m. The white thin line adjoining the black strip indicates however that the trailing edge of the propagating LAIW starts to evolve over the local topography obstruction in the area where the water depth is less than 250 m. One hour later (Figure 3b) the surface signature of the propagating LAIW reveals a remarkable spatial (x, y) anisotropy which is getting stronger over time. It is clear that the wavelength of the LAIW does not remain constant along the wave front. It increases up to 3 km in some places in the shallow water, whereas it remains unchanged in the deep part of the basin. Note also that a series of secondary dispersive waves starts to evolve at the trailing edge of the LAIW in the shallow water zone. This dispersion is clearly seen as a series of alternative white and black strips accompanying the trailing edge of the internal wave. This dispersion is getting stronger over time, and the dispersive wave tail occupies gradually increasingly larger areas (compare Figures 3b and 3c).

[25] In addition to dispersion, the wave refraction is also seen in Figure 3. It is clear that various fragments of the LAIW propagate in different background conditions (owing to the variations of water depth), and hence they have a different phase speed. As a result, the wave front is distorted, and the curvature of the wave front is dramatically increased over time (Figure 3c).

[26] The final stage in the process of wave transformation is the wave breaking. Wave disintegration can be traced in Figure 3 starting from Figure 3d. The latter shows the initial stage of the LAIW destruction, which is mostly completed 1 hour later (see Figure 3e). Figure 3f shows that the propagating wave is involved in breaking event except of the area at the right periphery of Figure 3 (between $x = 35$ and $x = 45$ km) where white strips can be treated as evidence of the changing polarity of incident LAIW.

[27] Summarizing this quick qualitative consideration, one can conclude that Figure 3 reveals several scenarios of wave shoaling depending on local bottom geometry. They are considered below in more detail on the basis of the analysis of wave patterns taken at different vertical cross sections. These sections are marked in Figures 3c at the bottom by arrows. The title of every scenario is given according to the basic effects occurring there.

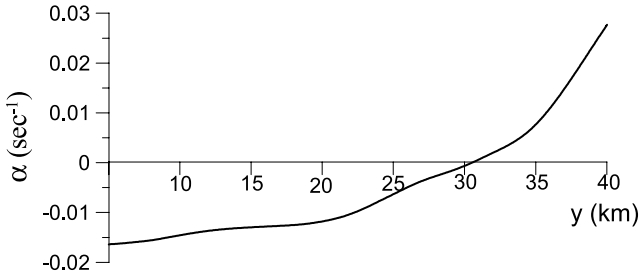

Figure 5. Coefficient of the quadratic nonlinearity α of the KdV equation calculated for section I.

3.1. Changing the Polarity and Dispersion

[28] Figure 4 represents the wave evolution along cross section I (see also Figure 3) which is characterized by a relatively smooth and gently sloping (almost monotonous) bottom profile. In a deep part of the basin (where H > 300 m) the propagating LAIW adjusts permanently to the varying bottom topography preserving its form in the course of propagation (the effect of adiabatic adjustment is discussed by *Vlasenko et al.* [2005a]). However, the existing balance between nonlinearity and dispersion is violated in the shallow part of the basin where depth H < 300 m, and the LAIW starts to disintegrate.

[29] In general, there are two extreme mechanisms of wave shoaling: dispersion and breaking. In the present particular case an average bottom inclination along cross section I is equal to 0.33° which can be considered as a minor value. In terms of the breaking criterion suggested by *Vlasenko and Hutter* [2002a], this case can be treated as a dispersive regime when breaking event does not happen, but solitary waves disintegrates into a packet of secondary short waves. Really, as it is seen in Figure 4a, the trailing edge of the LAIW is getting steeper at the first stage of distortion, and gradually transforms into the solitary wave of elevation. The rest of the energy of the incident LAIW is transformed into the attached dispersive wave tail.

[30] In fact, the process of wave evolution described above is qualitatively similar to that predicted by weakly nonlinear theory when internal wave changes its characteristics passing through the "turning point" where the coefficient of quadratic nonlinearity, α, i.e.,

$$\alpha = \frac{3c}{2}\frac{\int_{-H}^{0}(dq/dz)^3 dz}{\int_{-H}^{0}(dq/dz)^2 dz}$$

in the KdV equation changes its sign. Here c is the phase speed and $q(z)$ is the vertical profile of the first baroclinic mode defined from a standard boundary value problem. Figure 5 illustrates the dependence of the coefficient a on the horizontal coordinate calculated for section I (Figure 3). It is clear that the coefficient a changes its sign at the isobath of about 160 m. The change of sign from negative to positive implies that solitary internal waves of depression can not exist in shallow water zone "behind" the turning point where H < 160 m. The propagating solitary wave of depression must transform into solitary wave (or several waves) of elevation and attached dispersive wave tail. Exactly such a process is observed in Figure 4 with only one exception that the wave disintegration for LAIW starts earlier than that predicted by weakly nonlinear theory. As a result, the solitary wave of elevation has been already formed well before the turning point, see Figure 4d. The most possible reason of such early-stage transformation is that the incident LAIW produces strong depression of pycnocline in front of the propagating successive short internal waves so that the effective "turning point" is located much farther toward the deep water.

3.2. Dispersion and Breaking Accompanied by Energy Increase

[31] The evolution of the LAIW along section II reveals slightly different behavior (Figure 6) in comparison with that considered above, although they are very similar at the

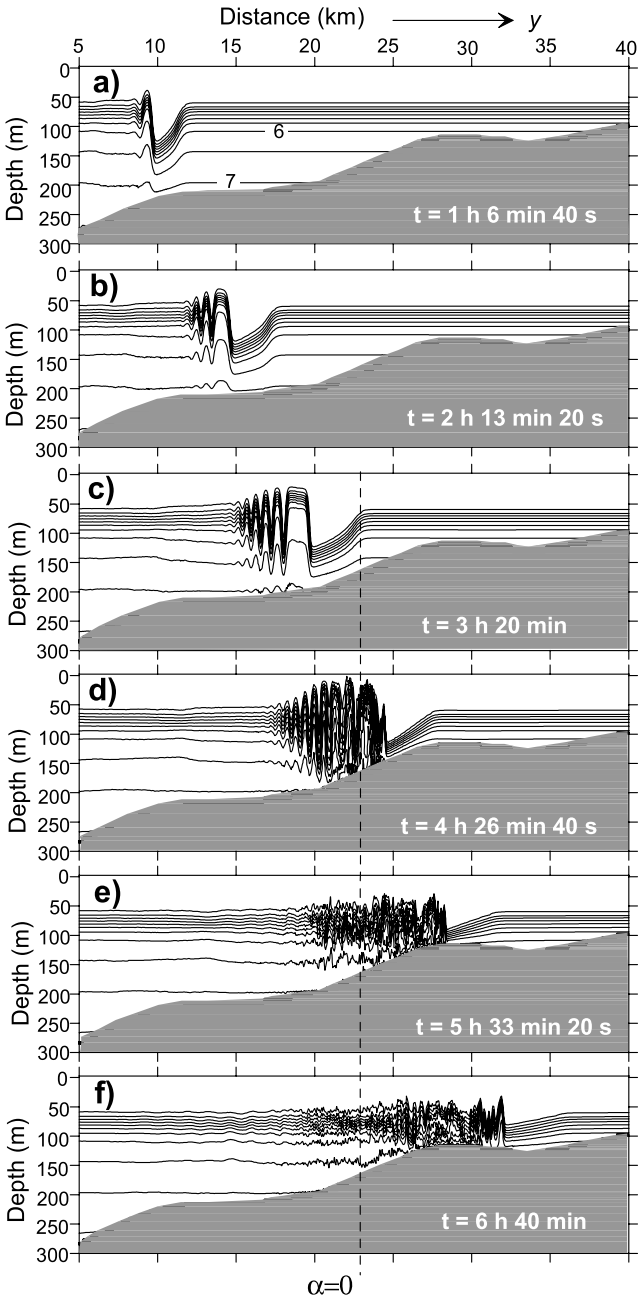

Figure 6. Same as in Figure 4 but for section II (see Figure 3).

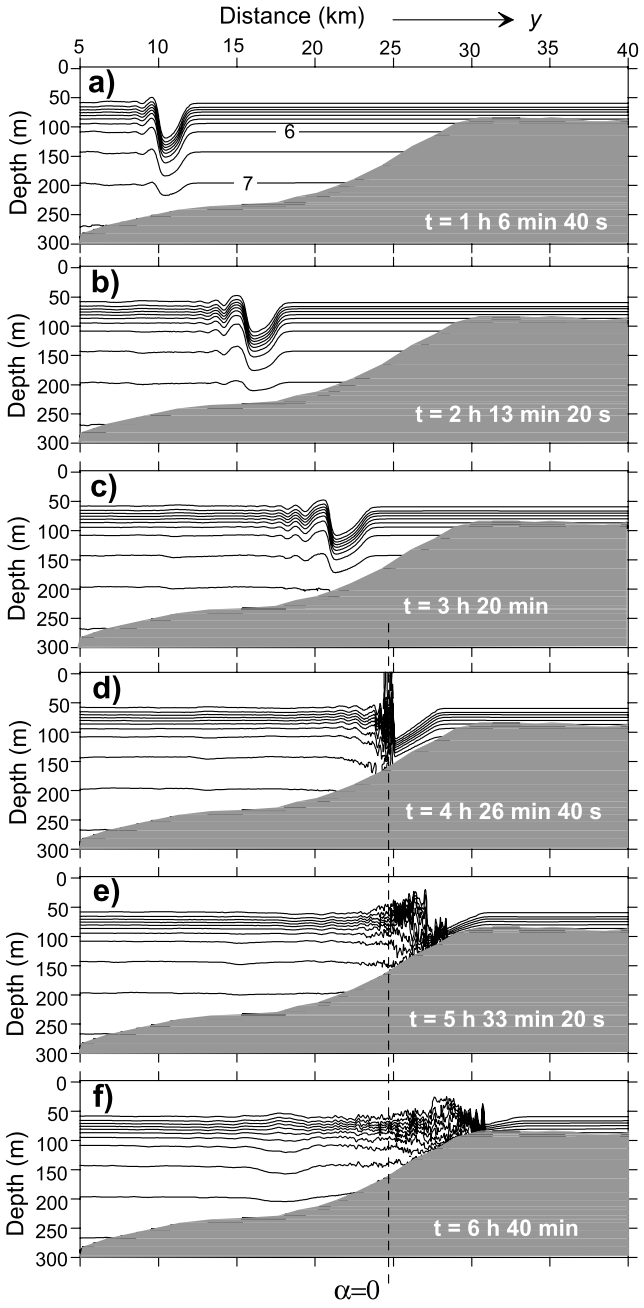

Figure 7. Same as in Figure 4 but for section III (see Figure 3).

first stage: the trailing edge of the LAIW starts to steepen in both cases with the formation of a packet of attached internal waves as it occurs in scenario I. Moreover, comparing the pairs, Figures 4d and 6b, (or Figures 4e and 6c) one can conclude that qualitatively they look very similar with the formation of a leading LAIW of elevation (even though well before the turning point, see explanation above) with the attached dispersive wave tail. The only difference between them is that the leading LAIW in Figure 6c is much stronger (a soliton of limited amplitude, in fact) than that in Figure 4d. This is an unexpected result taking into account that the leading wave in Figure 6c is located at a depth of about 200 m whereas in Figure 4c it propagated up to the 150-m isobath so that the waveguide in the last case is narrower and the energy concentration should be larger. It looks like the LAIW in Figure 6 gained some extra portion of energy; at the same time Figure 4 reveals evidence of energy loss. As we will see below, this is the case, and the reason for such energy redistribution along the wave front is discussed in the next section.

[32] The last remark about Figure 6 is that the leading internal wave of limited amplitude eventually breaks down in the vicinity of the 150-m isobaths (see Figures 6d and 6e) with the formation of a turbulent spot and several boluses propagating upstream (Figure 6f).

3.3. Dispersion and Breaking Accompanied by Energy Decrease

[33] The evolution of the LAIW along the cross section III (see Figure 3c) looks as if the wave is losing its energy in the coarse of its evolution (see Figure 7). Even though the bottom profile in Figures 6 and 7 are similar in general features, the wave shoaling in these two cross sections differs dramatically. In fact, initial weak dispersive disintegration observed in Figures 7b and 7c is suppressed by successive strong wave overturning and breaking of the steep trailing edge. In general, Figure 7 reveals that the wave packet is less energetic than that in Figure 6. The possible explanation of this obvious discrepancy might be the leakage of energy from the wave along the wave front in the adjacent areas. This mechanism is discussed in section 4.

3.4. Change of Polarity and Breaking

[34] Figure 8 represents the shoaling of the LAIW along cross section IV. A quick look at this series reveals that in many features it is similar to those presented in Figure 7. This similarity basically comes from the fact that in both cases the bottom profile is nearly similar. It includes three fragments: a gently sloping deep part of the slope (at $x < 20$ km in Figure 7 and $x < 25$ km in Figure 8), a steep middle part of the slope and a shelf. The only substantial difference is that the middle fragment in Figure 8 is not as steep as in Figure 7 so that shoaling LAIW has more time for evolution there. As a result, the propagating wave of depression transforms into the wave of elevation (Figure 8d) and only after that, breaks down in the swash area (Figure 8e). The final stage, i.e., the formation of a turbulent spot and its propagation shoreward (Figure 8f) is similar in both cases.

4. Comparison of 2-D and 3-D Models

[35] The comparison of wave evolution in sections II and III suggests an idea of possible transverse energy redistribution. It is clear that the wave refraction in the 3-D case leads to the localized changes in the curvature of the wave fronts. This effect, in turn, may cause the energy focusing in the places of localized bottom obstacles where wave fronts are usually concave and as a result of this fact the energy flux is directed toward the center of curvature. Such features of the oceanic bottom topography like banks or bottom headlands may work as ''optical lenses'' focusing the energy. In the opposite case of convex configuration of wave pattern the density of wave energy is normally less than that in the initial plane wave. The simplest way to illustrate this idea may obviously be obtained in the frame-

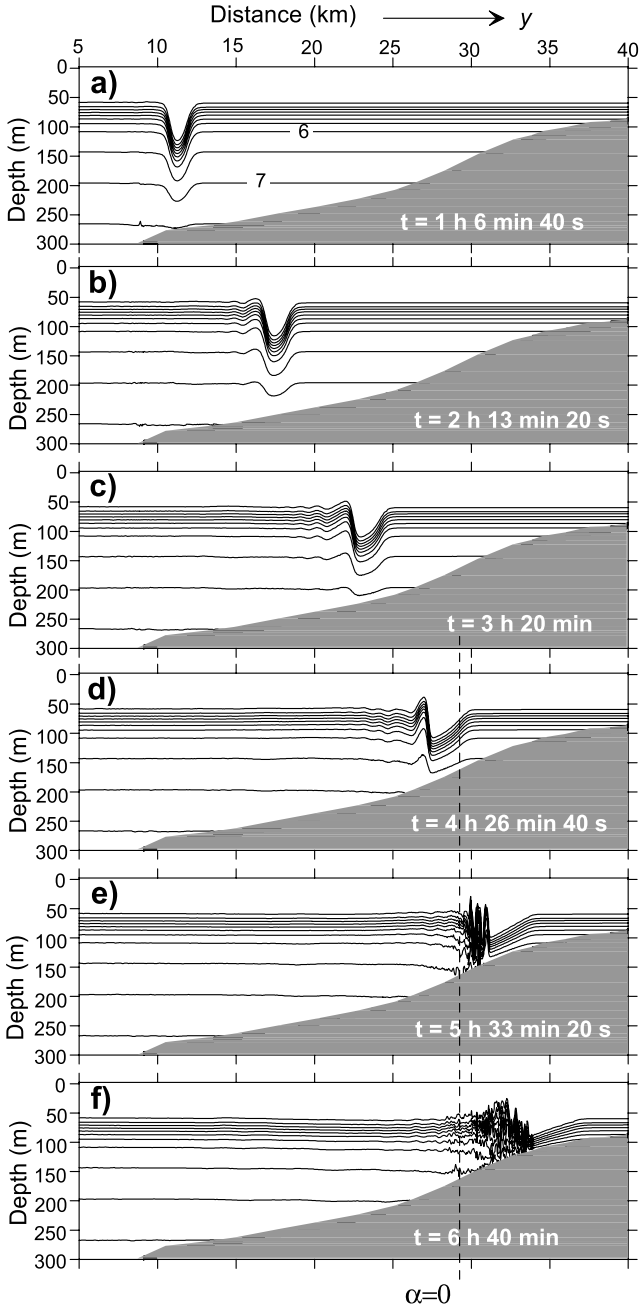

Figure 8. Same as in Figure 4 but for section IV (see Figure 3).

work of the theory of geometrical optics. Figure 9 represents a series of wave rays propagating initially perpendicular to the front of incident wave near the boundary of the computational domain. The trajectories of wave rays have been reconstructed using the geometrical optics equations [*Whitham*, 1974]. Input parameter in this problem was the linear wave speed of the first baroclinic mode calculated in every grid point. As it is clear from the analysis of Figure 9, the geometrical optics predicts energy focusing in the area of the headland marked by shaded ellipses where wave rays converge, whereas the rectangular areas are potential places of energy scattering because the divergence of the wave rays here is evident.

[36] This conclusions obtained in the framework of the linear approach, shows an expected wave evolution which may be valid also in the nonlinear case. Note, however, that the method of ray tracing (even being modified to account some nonlinear effects [*Small*, 2001a]) is inappropriate for description of the latest stages of wave shoaling when the processes of wave disintegration starts to develop (amplitude saturation, wave breaking, water mixing, relaxation). Thorough analysis of the wave profiles and energy balance presented below confirms this statement. The comparison of wave profiles presented in Figures 6 and 7 (wave shoaling along sections II and III) with the results of a 2D model where transverse derivatives $\partial/\partial x$ were equal to zero and where the energy flux of the incoming wave is constant in every cross section, underpins the idea about the energy focusing. A quick look at the wave evolution in section II and III presented in Figures 6 and 7 may lead to the conclusion that even though these two bottom profiles are very similar qualitatively, the process of wave shoaling along section II is more energetic than that along section III. This may be a possible confirmation of the effect of the energy redistribution discussed above, which leads to wave focusing over the bottom of headlands (section II; see Figure 3) and wave scattering along section III. An answer can be found from the analysis of Figures 10 and 11 where the comparison of 2-D and 3-D cases is presented. In the 2-D modeling scenario the bottom profile was the same as in sections II and III but without x variations of bottom topography. We restrict our analysis considering only one isopycnal, $\rho(z) - \rho(0) = 4$ kg m^{-3}, which makes our conclusion more obvious.

[37] The fact that the 3-D wave has an excess of energy along cross section II in comparison with the 2-D counterpart is evident from the analysis of Figure 10. The discrepancy between 2-D and 3-D waves becomes apparent from the moment when the wave front starts to distort owing to refraction in the area of the bathymetry adjacent the headland. This discrepancy between 2-D and 3-D wave profiles accumulates over time as long as the wave front is getting

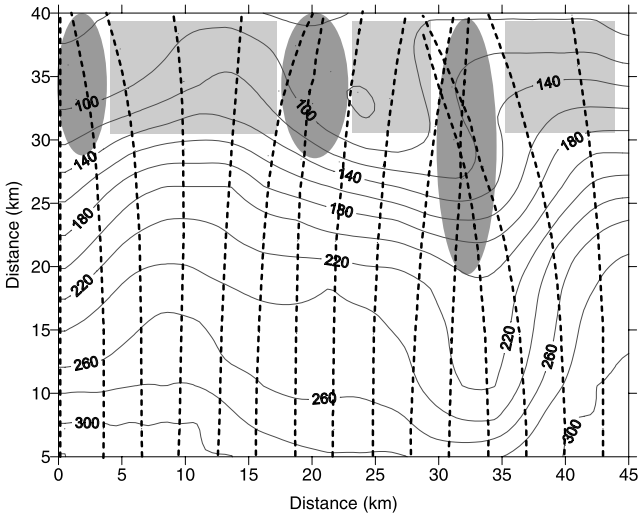

Figure 9. Pattern of the wave rays produced by a plane linear wave propagating through the studied area. Zones of focusing and scattering of the wave energy are presented by shaded ellipses and rectangles, respectively.

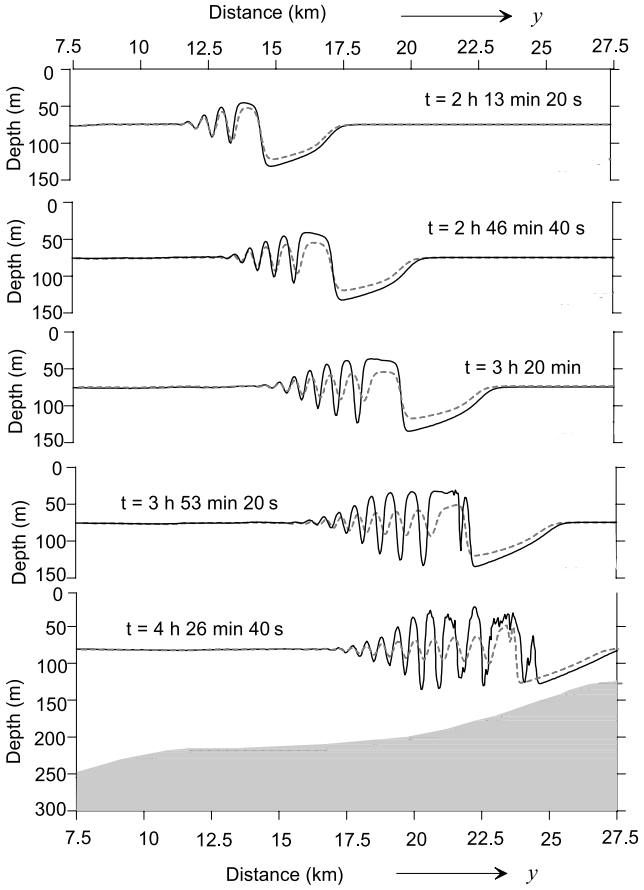

Figure 10. Time series of the reference isopycnal $\rho(z) - \rho(0) = 4$ kg m^{-3} presenting the evolution of a LAIW in section II (Figure 3). Solid lines represent 3-D model results; dashed lines were obtained in the framework of a 2-D model.

more concave. From the comparison of the solid and dashed lines it is seen that the difference in wave amplitude is almost twofold (see wave profiles at t = 4 hours 26 min). It is expected that the difference in wave energy is fourfold (for the analysis, see the next section).

[38] An opposite process occurs in cross section III where the shoaling 3-D internal wave loses more energy during the course of propagation in comparison with 2-D wave, as seen in Figure 11. The wave front of the 3-D wave in this section is convex owing to refraction (see Figure 3) which leads to the wave scattering and hence to the decrease of energy density (or energy flux) in this section. More detailed quantitative analysis of the effect of energy redistribution is performed below on the basis of the energy balance equations.

5. Balance of Wave Energy

[39] The wave energy, E, is a sum of the kinetic energy, E_{kin}, and the potential energy, E_{pot}, i.e., $E = E_{\mathrm{kin}} + E_{\mathrm{pot}}$. The total kinetic and potential energy integrated along the Oy axis from $y_1 = 0$ km to $y_2 = 45$ km per unit length in x direction can be written as

$$E_{\mathrm{kin}} = \int_{y_1}^{y_2}\int_{-H}^{\zeta} \rho \frac{(u^2+v^2+w^2)}{2}\,dzdy, \quad E_{\mathrm{pot}} = g\int_{y_1}^{y_2}\int_{-H}^{\zeta} \rho z dzdy.$$

The expression for the potential energy, E_{pot}, can be rewritten in terms of available potential energy taking into account that the internal wave displaces the isopycnal from its stationary depth of equilibrium, z^*, to the disturbed level, z. If so, E_{pot} can be presented as a sum of the background potential energy, E_{bg}, and the available potential energy, E_{ape}, as follows $E_{\mathrm{pot}} = E_{\mathrm{bg}} + E_{\mathrm{ape}}$, where

$$E_{\mathrm{bg}} = g\int_{y_1}^{y_2}\int_{-H}^{\zeta} \rho z^* dzdy, \quad E_{\mathrm{ape}} = g\int_{y_1}^{y_2}\int_{-H}^{\zeta} \rho(z-z^*)\,dzdy.$$

It is clear that E_{bg} does not depend on the parameters of the incoming wave. It describes only the potential energy due to the background stratification. If so, this term can be omitted as an additive constant. Thus the integrated total energy of the internal wave per unit length along the Oy axis in the Ox direction reads

$$E = E_{\mathrm{kin}} + E_{\mathrm{ape}}. \tag{1}$$

The difference between the initial energy of the incident wave, E_0, calculated at $t = 0$ and its current value, $E(t)$, shows

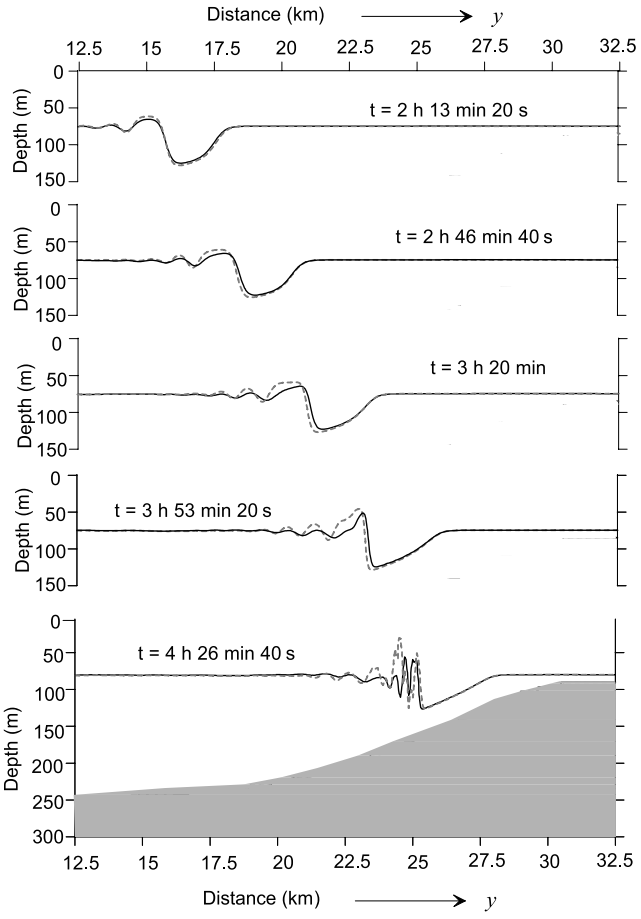

Figure 11. Same as in Figure 8 but for section III (see Figure 3).

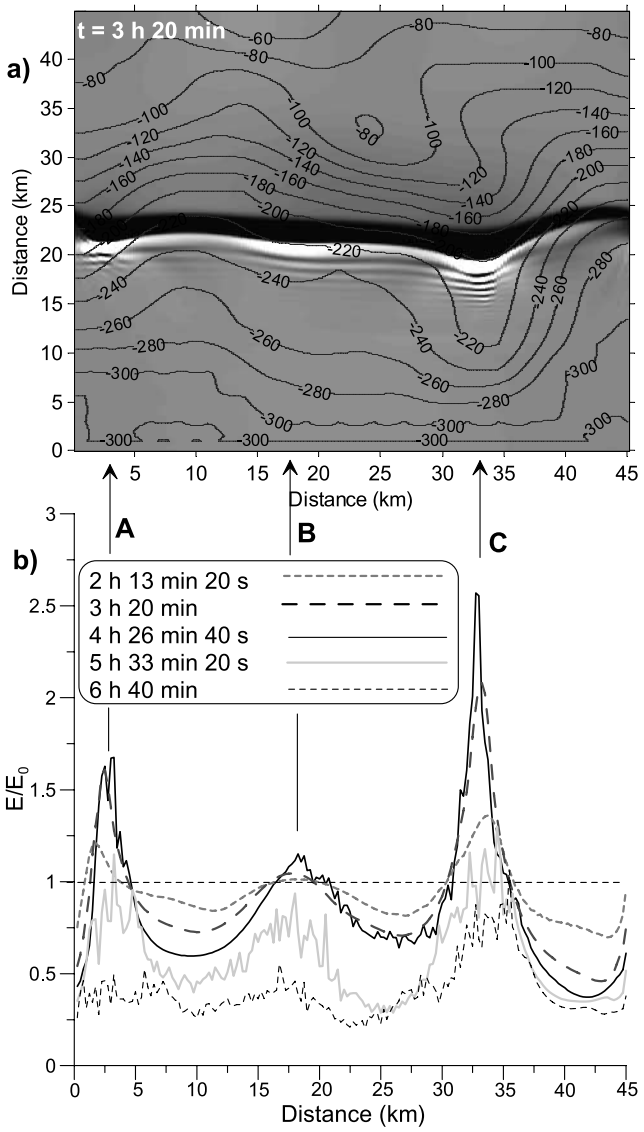

Figure 12. (a) Sea surface topography produced by a shoaling LAIW overlaid with bathymetric map. Elevations and depressions are shown by black and white colors, respectively. (b) Dependence of the total wave energy integrated over (y, z) on the x coordinate. The energy is normalized by its initial value at $t = 0$.

how much energy has been lost during the course of wave propagation. Energy dissipation in the bottom boundary layer and the density jump before the breaking event, and water mixing during wave breaking in the swash zone provide the principal sink of wave energy. Another possible process which may develop during the wave shoaling is the energy redistribution discussed above. As it was shown, the wave refraction may lead either to energy focusing or wave scattering. The example presented below is the best illustration of this effect.

[40] Figure 12 shows the distribution of the integrated wave energy, $E(x,t)$, in section (y,z) normalized by its initial value, E_0, calculated at $t = 0$. Figure 12 (top) showing the sea surface elevation of the LAIW at $t = 3$ h 20 min with overlaid bottom topography is presented here for better illustration of the effect of wave refraction. The initial normalized value of energy is shown by the horizontal dotted line $E/E_0 = 1$.

[41] The analysis of the $E(x,t)/E_0$ profiles taken at different moments of wave shoaling reveals an effect of redistribution of wave energy along the wave front. The three peaks marked by letters A, B and C identify the area with an excess of wave energy in comparison with its initial value. As is clear from Figure 12, the energy accumulates over time in the region of wave focusing. Scrutiny of the $E(x,t)/E_0$ curves and their correlations with the bottom topography indicates that the energy is accumulated in the areas of the bathymetry adjacent headlands where the wave front has a concave profile due to refraction. We can expect also that the energy focusing must be more effective at locations with larger bottom curvature. As a confirmation, the energy peak over headland C is larger than that in areas A and B.

[42] Note that the energy focusing develops on the background of two other effects. As it follows from the principle of energy conservation, an excess of energy in one site of the wave field inevitably leads to a deficit in adjacent areas. This effect is clearly seen in Figure 12. Another process which should be taken into account is the energy dissipation due to viscosity, especially in the areas of wave breaking. As confirmation, Figure 12 reveals that after 5 hours of wave shoaling the normalized energy of the LAIW becomes essentially smaller in comparison with the initial value. The main part of the wave energy is dissipated in the swash zone where strong mixing processes take place (see also Figures 6–8). To estimate the total energy loss in the whole domain we should calculate the integrals $\tilde{E}_{\mathrm{kin}} = \int_{x1}^{x2} E_{\mathrm{kin}} dx$, $\tilde{E}_{\mathrm{ape}} = \int_{x1}^{x2} E_{\mathrm{ape}} dx$ in the interval between $x_1 = 0$ km and $x_2 = 45$ km (see Figure 12).

[43] Figure 13 shows the percentage of the kinetic energy (thin line), available potential energy (dashed line) and the total energy (thick line) integrated through the whole water column. An appropriate initial value at $t = 0$ was taken as 100%. It is clear from Figure 13 that the rate of energy dissipation is not constant over time, but changes dramatically during the wave shoaling. Scrutiny of the presented

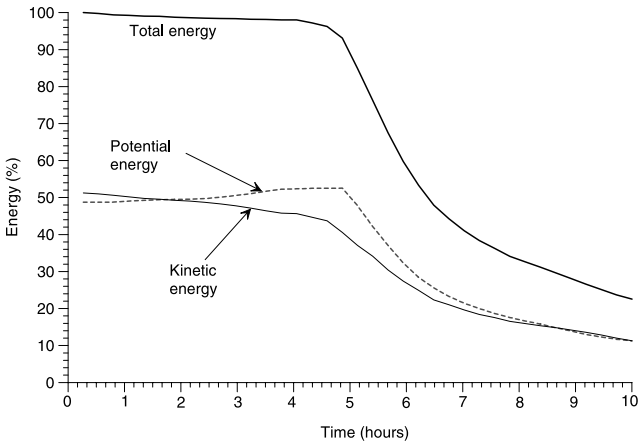

Figure 13. Dependence of the kinetic energy (thin line), potential energy (dashed line), and their sum (thick line) on time during the evolution of LAIW normalized by initial value of energy.

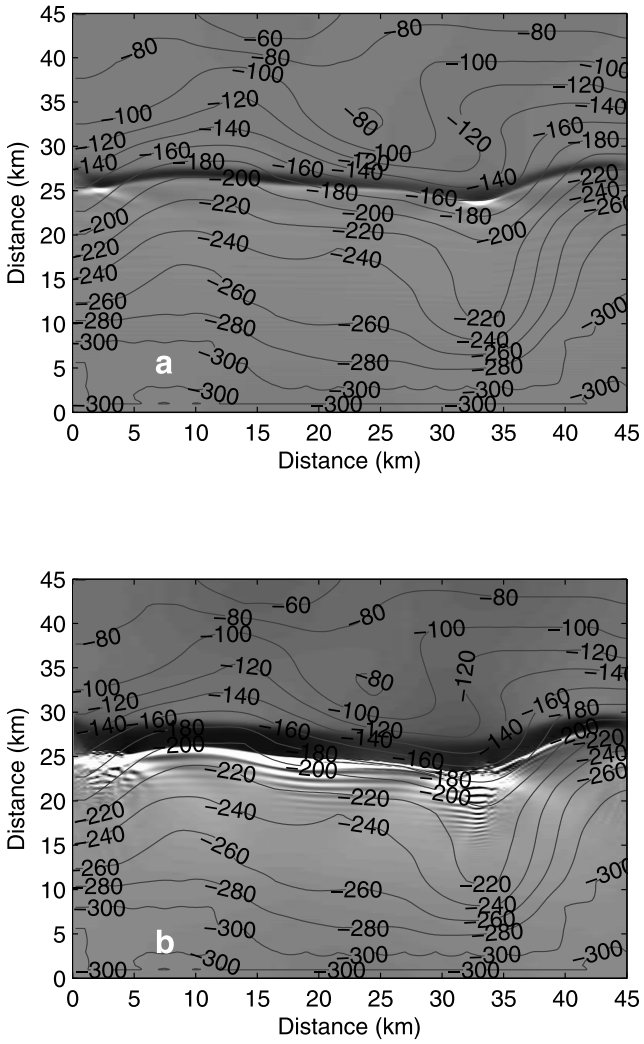

Figure 14. Sea surface topography produced by LAIWs with amplitudes (a) 25 m and (b) 81 m at $t = 4$ hours 26 min. Surface elevations and depressions are shown by black and white, respectively.

dependencies allows one to conclude that the LAIW gradually loses its energy at the first stage of evolution (during first 4 hours), but this process may be identified as moderately weak attenuation. The main process which is responsible for the energy decay is the dissipation in the bottom boundary layer. Note also that the potential energy actually slowly increases during the course of wave evolution, which takes place owing to the gradual increase of wave amplitude during shoaling.

[44] Similar effects continue to develop during the next hour (from 4 hours to 4 hours 50 min) although the initial stage of wave breaking in the area of the bathymetry adjacent the headland turns the weak attenuation into a more dramatic energy decay.

[45] The next stage of wave evolution is characterized by strong wave breaking which almost develops across the entire computational domain. This is the reason why the propagating LAIW loses almost half of its energy from 4 hours 50 min to 6 hours 20 min owing to the mixing and dissipation. Finally, after 6–7 hours of shoaling the incoming LAIW disintegrates into a large number of wave fragments (see Figure 3f) and strong wave breaking transforms it into a viscous evolution of secondary short waves.

6. Sensitivity Runs

[46] The results presented above illustrate how strong the shoaling scenario depends on 3D characteristics of the bottom profile. Being obtained for the wave with amplitude of 69 m, this tendency remains valid in a wide range of wave intensity. This section focuses on the sensitivity of the shoaling process to the amplitude of incident wave.

[47] Figure 14 shows a plan view of the sea surface elevation produced by propagating internal wave with initial amplitude of 25 m (Figure 14a) and 81 m (Figure 14b). All designations here are similar to those in Figure 3 where incident LAIW has the amplitude of 69 m. The comparison analysis of these two patterns gives rise to the conclusion that the weaker waves are able to penetrate farther into shallow water without remarkable dispersion and breaking. At least the wave front in Figure 14a looks like that produced by a single solitary wave except maybe two fragments where white spots can be interpreted as secondary waves of elevation. As distinct from weak wave, the large wave presented in Figure 14b has already disintegrated into multiple secondary waves in the same place of topography. Surprisingly, that the wave refraction is not

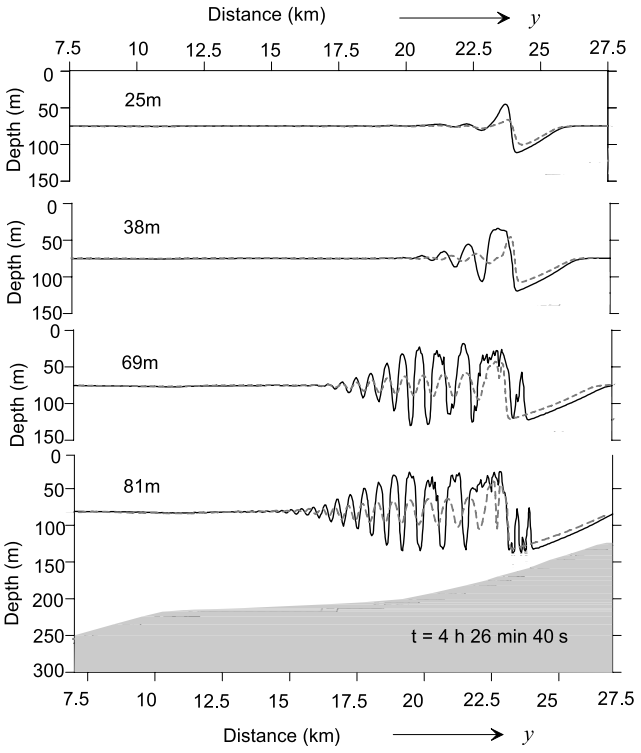

Figure 15. Profiles of the reference isopycnal $\rho(z) - \rho(0) = 4$ kg m^{-3} produced by LAIWs with amplitudes 25 m, 38 m, 69 m, and 81 m at the same moment of time in section II (see Figure 3). Solid lines represent 3-D model results; dashed lines were obtained in the framework of a 2-D model.

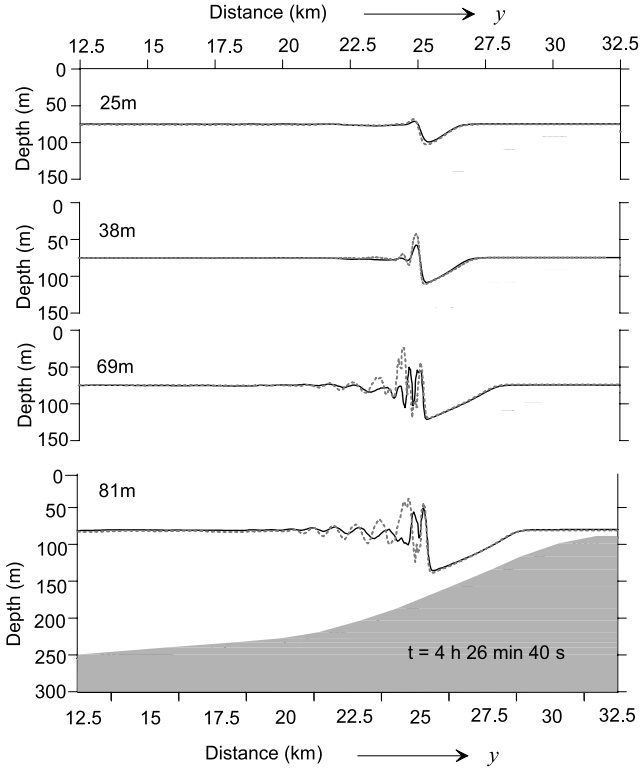

Figure 16. Same as in Figure 15 but for section III (see Figure 3).

sensitive to the wave amplitude. The most probable reason for this effect is that the nonlinear dispersion (the dependence of phase speed on wave's amplitude) is a second-order effect in comparison with the spatial variability of the phase speed due to the depth variations. As a confirmation, the shape of wave fronts in both cases looks very similar for large and small waves. More clearly the effects of amplitude on the wave shoaling can be studied considering of wave profiles in different cross-shelf sections.

[48] Figure 15 shows several wave profiles above the slope in section II produced by the incoming waves with amplitudes of 25, 38, 69 and 81 m. Solid lines represent the 3-D case whereas dashed lines correspond to 2-D version of the model. Scrutiny of Figure 15 shows that the effect of energy redistribution along the wave front over complex 3-D topography takes place for all considered amplitudes. Even in a weakly nonlinear case (Figure 15, top) the incident wave with amplitude of 25 m evolves differently in 2-D and 3-D cases. As a result of the energy focusing its amplitude increased dramatically (more than 2 times in the rear fragment of elevation). Similar tendency is also valid for the medium- and the large-amplitude waves. In the last case (presented for the wave with amplitude of 81 m in Figure 15, bottom) the process of wave shoaling and amplification due to energy focusing is similar to that formulated in the previous section, but the discrepancy between 2-D and 3-D waves is stronger.

[49] The effect of the energy dispersion described above occurring in the areas of local canyons, is also inherent to all considered waves. This is clearly seen in Figure 16 where four wave profiles for incident waves with amplitudes of 25, 38, 69 and 81 m are shown in the cross section III (see Figure 3). Note that the effect of energy scattering here is more evident for the large-amplitude waves rather than for the small ones.

[50] Similar conclusion can be also formulated for the dependence of wave attenuation on amplitude of shoaling wave. Figure 17 illustrates that 81-m amplitude LAIW loses about 60% of its energy after 6 hours of evolution whereas 25-m internal wave preserves almost half of its initial energy even after 10 hours of shoaling. It is clear from the previous analysis that stronger waves start to disintegrate earlier (see Figures 15 and 16). This disintegration includes both dispersive fission and wave breaking when dissipative effects are especially pronounced and energy consuming. As a result, weaker waves penetrate much farther into the shallow water zone without breaking.

7. Summary and Conclusions

[51] Oceanic nonlinear internal waves are widely acknowledged as being a small-scale process with global and climatic significance. Breaking of internal waves is a key process in setting the density structure of the Global Ocean, and hence the density driven circulation. The transport of mass produced by the LAIWs also has important ecological implications not only because the LAIWs may transport nutrients and plankton, but also because they can lead to accumulation, transport and/or retention of plankton. The mixing produced by internal waves can drive a supply of nutrients from the high-nutrient waters in the abyss into the frequently nutrient depleted surface layer.

[52] We present here a series of numerical experiments performed with the aim of reproducing a 3-D shoaling of large-amplitude internal waves focusing on the more critical stage of their evolution, i.e., disintegration, breaking and associated turbulent mixing. Greater insight into the strongly nonlinear dynamics and energetics of the LAIWs in slope-shelf areas in general, and the swash zone in particular, is achieved with the use of a state-of-the-art 3-D nonhydrostatic numerical model. In combination with sea surface SAR images this model has permitted the 3-D description + quantification of wave shoaling providing a greater insight

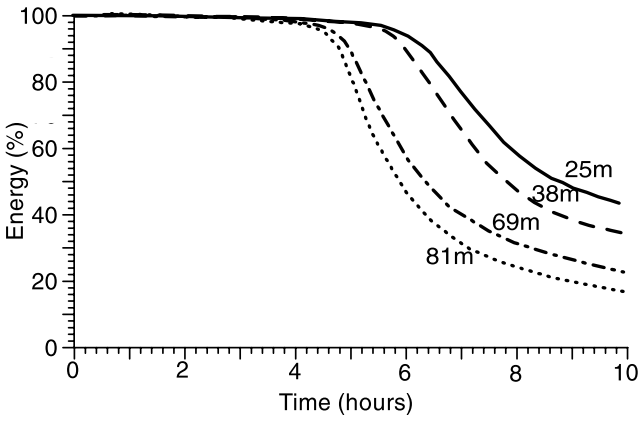

Figure 17. Dependence of the normalized total energy of LAIWs on the time of evolution for different wave amplitudes.

into the physical processes involved as compared with the traditional approach of looking at the LAIWs as a 2-D and weakly nonlinear problem.

[53] The vertical fluid stratification, the parameters of the propagating LAIWs as well as the bottom profile presenting essential 3-D structure within the vicinity of the headlands and canyons, were taken close to those observed in the northern part of the Andaman Sea. An accurate prediction of the baroclinic fields produced by the incoming LAIWs in the chosen part of shelf-slope area was generated with the use of the MITgcm. All important stages of the 3-D shoaling of LAIW, including the initial adiabatic adjustment in the deep part of the ocean, successive transformation and disintegration over the continental slope, final breaking and water mixing in a swash zone were reproduced by the model.

[54] It was found that from a first glance many general features of wave shoaling in three dimensions look similar to those occurring in a 2-D case. This relates first of all to the qualitative behavior of LAIWs over an inclined bottom. Wave disintegration, steepening and breaking may be described in a similar way as per 2-D waves [see, e.g., *Vlasenko and Hutter*, 2002a, 2002b]. However, the 3-D process of wave shoaling differs from a 2-D evolution in many quantitative characteristics which have some important implications. First of all, it was found that the process of wave refraction developing in the areas of local bottom elevations or depressions in a 3-D case produces concave or convex fragments of the wave fronts. This, in turn, leads to the transverse redistribution of energy along the wave fronts. Scrutiny of the energy characteristics of the propagating LAIWs has shown that concave wave fragments work as optical lenses focusing the wave energy to the centers of curvature. This effect, being less remarkable for small-amplitude waves, is highly important for LAIWs. Indeed, in a shallow water zone where LAIWs have their amplitude close to the limiting value, the breaking event develops faster if there is an extra source of energy. Wave focusing provides such an extra source. In a general oceanographic context, it should be expected to find spots of higher levels of turbulent kinetic energy (TKE) in the areas of local banks and headlands. In this respect the situation with bottom depressions is quite opposite: these areas should be potential places with low level of TKE.

[55] The obtained results relate directly to the predictability of the vertical and horizontal transport of dissolved chemical elements and suspended matter in shelf-slope areas and may thereby assist in assessing the impact of LAIWs on the ecosystem. Although obtained for the conditions of the Andaman Sea, the basic finding from this study can be easily used for interpretation of SAR images revealing shoaling of oceanic internal waves in many other shelf-slope areas.

[56] **Acknowledgment.** We thank Nigel Aird for his helpful discussions.

References

Alpers, W., H. Wang-Chen, and L. Hock (1997), Observation of internal waves in the Andaman Sea by ERS SAR, paper presented at Third ERS Symposium on Space at the Service of our Environment, Eur. Space Agency, Florence, Italy.

Choi, W., and R. Camassa (1999), Fully nonlinear internal waves in a two-fluid system, *J. Fluid Mech.*, *396*, 1–36.

Egbert, C. D., and R. D. Ray (2001), Estimates of M_2 tidal energy dissipation from TOPEX/POSEIDON altimeter data, *J. Geophys. Res.*, *106*(C10), 22,475–22,502.

Fraser, N. (1999), Surfing an oil rig, *Energy Rev. Feb/Mar*, 20–24.

Grimshaw, R. (1985), Evolution equations for weakly nonlinear, long internal waves in rotating fluid, *Stud. Appl. Math.*, *73*, 1–33.

Grimshaw, R., and S. Tang (1990), The rotation-modified Kadomtsev-Petviashvili equation: An analytical and numerical study, *Stud. Appl. Math.*, *83*, 223–248.

Grimshaw, R., E. Pelinovsky, and T. Talipova (1997), The modified Korteweg-de Vries equation in the theory of large amplitude internal waves, *Nonlinear Processes Geophys.*, *4*, 237–250.

Helfrich, K. R., and W. K. Melville (2006), Long nonlinear internal waves, *Annu. Rev. Fluid Mech.*, *38*, 395–425.

Helfrich, K. R., and J. Pineda (2003), Accumulation of particles in propagating fronts, *Limnol. Oceanogr.*, *48*, 1509–1520.

Holloway, P. E., E. N. Pelinovsky, and T. Talipova (1999), A generalized Korteweg-de Vries model of internal tide transformation in the coastal zone, *J. Geophys. Res.*, *104*(C8), 18,333–18,350.

Jackson, C. R. (2004), An atlas of internal solitary-like waves and their properties, report, Global Ocean Assoc., Alexandria, Va. (Available at http://www.internalwaveatlas.com/Atlas2_PDF/IWAtlas2_FrontMatter.pdf)

Lamb, K. G. (2002), A numerical investigation of solitary internal waves with trapped cores formed via shoaling, *J. Fluid Mech.*, *451*, 109–144.

Lamb, K. G. (2003), Shoaling solitary internal waves: On criterion for the formation of waves with trapped cores, *J. Fluid Mech.*, *478*, 81–100.

Leichter, J. J., H. L. Stewart, and S. L. Miller (2003), Episodic nutrient transport to Florida coral reefs, *Limnol. Oceanogr.*, *48*, 1394–1407.

Lennert-Cody, C. E., and P. J. S. Franks (1999), Plankton patchiness in high-frequency internal waves, *Mar. Ecol. Prog. Ser.*, *186*, 59–66.

Lennert-Cody, C. E., and P. J. S. Franks (2002), Fluorescence patches in high-frequency internal waves, *Mar. Ecol. Prog. Ser.*, *235*, 29–42.

Levitus, S., and T. P. Boyer (1994a), *World Ocean Atlas 1994*, vol. 4, *Temperature*, *NOAA Atlas NESDIS* 4, 129 pp., NOAA, Silver Spring, Md.

Levitus, S., and T. P. Boyer (1994b), *World Ocean Atlas 1994*, vol. 3, *Salinity*, *NOAA Atlas NESDIS* 4, 111 pp., NOAA, Silver Spring, Md.

Marshall, J., A. Adcroft, C. Hill, L. Perelman, and C. Heisey (1997), A finite-volume, incompressible Navier-Stokes model for studies of the ocean on parallel computers, *J. Geophys. Res.*, *102*(C3), 5753–5766.

Miyata, M. (1985), An internal solitary waves of large amplitude, *Mer*, *23*, 43–48.

Miyata, M. (1988), Long internal waves of large amplitude, in *Nonlinear Internal Waves*, edited by K. Horikawa and H. Maruo, pp. 399–406, Springer, New York.

Ostrovsky, L. A., and J. Grue (2003), Evolution equation for strongly nonlinear internal waves, *Phys. Fluids*, *15*, 2934–2948.

Ostrovsky, L. A., and V. I. Shrira (1976), Instability and self-refraction of solitons, *Sov. Phys. JETP, Engl. Transl.*, *44*, 738–743.

Ostrovsky, L. A., and Y. A. Stepanyants (1989), Do internal solitons exist in the ocean?, *Rev. Geophys.*, *27*, 293–310.

Pacanowski, R. C., and S. G. H. Philander (1981), Parametrisation of vertical mixing in numerical models of tropical oceans, *J. Phys. Oceanogr.*, *11*, 1443–1451.

Pineda, J. (1999), Circulation and larval distribution in internal tidal bore warm fronts, *Limnol. Oceanogr.*, *44*, 1400–1414.

Small, J. (2001a), A nonlinear model of the shoaling and refraction of interfacial solitary waves in the ocean. Part I: Development of the model and investigations of the shoaling effect, *J. Phys. Oceanogr.*, *31*, 3163–3183.

Small, J. (2001b), A nonlinear model of the shoaling and refraction of interfacial solitary waves in the ocean. Part II: Oblique refraction across a continental slope and propagation over seamount, *J. Phys. Oceanogr.*, *31*, 3184–3199.

Stanton, T. P., and L. A. Ostrovsky (1998), Observations of highly nonlinear solitons over the continental shelf, *Geophys. Res. Lett.*, *25*, 2695–2698.

Thorpe, S. A. (1987), On the reflection of a train of finite amplitude internal waves from a uniform slope, *J. Fluid Mech.*, *178*, 279–302.

Thorpe, S. A. (1997), On the interaction of internal waves reflecting from slope, *J. Phys. Oceanogr.*, *27*, 2072–2078.

Thorpe, S. A. (2000), The effect of rotation on the nonlinear reflection of internal waves from slope, *J. Phys. Oceanogr.*, *30*, 1901–1909.

Vlasenko, V., and K. Hutter (2002a), Numerical experiments on the breaking of solitary internal waves over a slope-shelf topography, *J. Phys. Oceanogr.*, *32*, 1779–1793.

Vlasenko, V., and K. Hutter (2002b), Transformation and disintegration of strongly nonlinear internal waves by topography in stratified lakes, *Ann. Geophys.*, *20*, 2087–2103.

Vlasenko, V., L. Ostrovsky, and K. Hutter (2005a), Adiabatic behavior of strongly nonlinear internal waves in slope-shelf areas, *J. Geophys. Res.*, *110*, C04006, doi:10.1029/2004JC002705.

Vlasenko, V., N. Stashchuk, and K. Hutter (2005b), *Baroclinic Tides: Theoretical Modeling and Observational Evidence*, 351 pp., Cambridge Univ. Press, New York.

Whitham, G. B. (1974), *Linear and Nonlinear Waves*, 656 pp., John Wiley, Hoboken, N. J.

N. Stashchuk and V. Vlasenko, School of Earth, Ocean and Environmental Sciences, University of Plymouth, Drake Circus, Plymouth PL4 8AA, UK. (nstashchuk@plymouth.ac.uk; vvlasenko@plymouth.ac.uk)